

Experimental free-space quantum key distribution over a turbulent high-loss channel

Md Mehdi Hassan

Department of Physics and Astronomy
The University of Tennessee
Knoxville, TN, USA
mhassal1@vols.utk.edu

Kazi Reaz

Department of Physics and Astronomy
The University of Tennessee
Knoxville, TN, USA
kreaz@vols.utk.edu

Adrien Green

Department of Physics and Astronomy
The University of Tennessee
Knoxville, TN, USA
agreen91@vols.utk.edu

Noah Crum

Department of Physics and Astronomy
The University of Tennessee
Knoxville, TN, USA
ncrum@vols.utk.edu

George Siopsis

Department of Physics and Astronomy
The University of Tennessee
Knoxville, TN, USA
siopsis@tennessee.edu

Abstract—Free-space quantum cryptography plays an integral role in realizing a global-scale quantum internet system. Compared to fiber-based communication networks, free-space networks experience significantly less decoherence and photon loss due to the absence of birefringent effects in the atmosphere. However, the atmospheric turbulence contributes to deviation in transmittance distribution, which introduces noise and channel loss. Several methods have been proposed to overcome the low signal-to-noise ratio. Active research is currently focused on establishing secure and practical quantum communication in a high-loss channel, and enhancing the secure key rate by implementing bit rejection strategies when the channel transmittance drops below a certain threshold. By simulating the atmospheric turbulence using an acousto-optical-modulator (AOM) and implementing the prefixed-threshold real-time selection (P-RTS) method, our group performed finite-size decoy-state Bennett-Brassard 1984 (BB84) quantum key distribution (QKD) protocol for 19 dB channel loss. With better optical calibration and efficient superconducting nano-wire single photon detector (SNSPD), we have extended our previous work to 40 dB channel loss characterizing the transmittance distribution of our system under upper moderate turbulence conditions.

Index Terms—quantum key distribution, QKD, BB84, free space QKD, quantum communication, channel loss, turbulence.

I. INTRODUCTION

Over the course of a year, the number of qubits in the most powerful quantum computers has tripled from 127 to 433. As engineering and technological capabilities keep increasing, the exponential growth of the number of qubits in quantum computers is inevitable. The relevance of switching from traditional modern encryption to quantum computer-proof data encryption is evident.

This material is based upon work supported by the Department of Energy, Office of Science, Office of Advanced Scientific Computing Research, through the Quantum Internet to Accelerate Scientific Discovery Program under Field Work Proposal 3ERKJ381. We acknowledge support by the National Science Foundation under grant DGE-2152168.

Quantum key distribution (QKD) offers absolute security for distribution encryption keys between two parties against eavesdropping by relying on the principles of quantum mechanics. Since the proposal of the very first quantum key distribution by Bennett and Brassard in 1984 (BB84) [1], numerous improvements have been made to this kernel, enabling its transition from theory to practical use. The first successful experimental prototype of BB84 [2] was announced in 1989, affirming 32 cm free-space data transmission that exploited the polarization property of light particles (photons). The experiment was done using incoherent green light (550 nm) as the source and photo multiplier tubes as the detectors.

In [1], the authors addressed the technical difficulties of producing consistent light pulses containing single photons, and proposed coherent or incoherent sources for light pulses. Processes to create single photons, such as through spontaneous parametric down conversion [3] or quantum dots [4], are expensive and still under active research. Meanwhile, coherent state implementations generate signals at a high rate and utilize cheaper off-the-shelf equipment [5]. Because of its practicality and high secure key rates, BB84 with weak coherent states has been the subject of extensive research and development. An important concern has been the fact that coherent states may contain multiple photons, which an eavesdropper can remove and copy through a Photon Number Splitting (PNS) attack [6]. To thwart such attacks, the decoy state method was invented [7] allowing communicating parties to monitor whether or not Eve has changed the photon number statistics of the light pulses. Over the years, security proofs have become more sophisticated in order to account for an increasing amount of details related to real implementations, such as the finite size effect [8] and the consideration of various side channel and individual attacks [9]. Today, QKD protocols encoded on weak coherent states have well established security proofs, high data rates and have been implemented in a number of

environments [10], [11], [12], [13]. While fiber based networks have seen significant improvements over the last few decades, however, transmission losses in standard fiber scale as ~ 0.2 dB/km at the telecom wavelength (~ 1550 nm) [14], and thus the systems are only viable at the intra-metropolitan scale [9]. Therefore, for longer distance secure communication such as a global scale quantum network, free space quantum channels are essential.

Some of the main challenges of free space communication are due to the effects of atmospheric turbulence. Even though the signal can propagate almost without attenuation in the upper atmosphere, the lower levels, especially the troposphere and stratosphere, degrade the intensity of the signal. For example, at an altitude of 1,200 km, the estimated loss due to atmospheric absorption and turbulence ranges between 3 and 8 dB [15], [16]. The variation in air temperature and pressure gradients with respect to position results in eddy flows of air, which cause changes in the refractive index over time and across different locations [17]. This results in beam front deformation and beam wandering, which affects the transmittance.

In this experiment, we simulate finite-key, polarization encoded BB84 with weak laser pulses with cutting edge detectors in a turbulent, high loss, free-space environment. Since atmospheric turbulence can be measured with a classical laser probe, resulting transmittance information can be used to reject groups of coherent states that are most likely to have suffered high loss. Detections that occurred during those time intervals are more likely to be detector noise than the signal and can be rejected to lower the average quantum bit error rate. In [18], it was argued that the cutoff is dependent only on device parameters rather than channel statistics, meaning that an optimal threshold can be prefixed, reducing data storage and computational requirements, which we investigate experimentally.

II. THEORY

In this section, we discuss the relationship between a turbulent atmosphere with finite key decoy state parameters for BB84, and the resulting effects to the secure key rate.

A. Atmospheric Effect

Atmospheric turbulence causes random transmittance fluctuations that can be modeled by a log-normal probability distribution [19] whose density function is given by

$$p_{\eta_o, \sigma}(\eta) = \frac{1}{\sqrt{2\pi\sigma\eta}} \exp\left\{-\frac{[\ln(\frac{\eta}{\eta_o}) + \frac{\sigma^2}{2}]^2}{2\sigma^2}\right\}, \quad (1)$$

where η_o is the average channel transmittance and the variance, σ^2 , gives the level of turbulence. σ^2 is commonly referred to as the Rytov parameter. If the transmitter and the receiver are separated by a horizontal distance L , the Rytov parameter is given approximately by the expression $\sigma^2 = 1.23 C_n^2 k^{\frac{7}{6}} L^{\frac{11}{6}}$ for plane waves with wave number k [20]. Here, C_n^2 is the refractive index structure parameter and n is the refractive index of the medium. The structure parameter varies depending on

altitude and temperature as well [21]. For example, $\sigma^2 = 0.924$ corresponds to both a small turbulence of $C_n^2 = 10^{-17} \text{ m}^{-\frac{2}{3}}$ covering air to air 100 km distance [22] as well as a higher turbulence of $C_n^2 = 6.2 \times 10^{-15} \text{ m}^{-\frac{2}{3}}$ covering a distance of 3 km.

In our experiment, a fiber-coupled acousto-optic modulator (AOM) was used to vary the photon intensity according to our desired transmittance model. We emulated the log-normal distribution (1) of the output signal via controlling the AOM device by an arbitrary waveform generator (AWG3). The turbulence parameter σ^2 was set to 1, which corresponds to upper-medium turbulence.

Nomenclature

N	Total pulse sent to Bob
R	Key rate
ℓ	Number of distilled secure bits
ϕ_x	Phase error
e_{obs}	Observed error
η	Channel transmittance
η_d	Detector efficiency
μ_i	Average photon number per pulse
q_x	Alice's probability of choosing \boxplus basis
q_z	Alice's probability of choosing \boxtimes basis
P^{μ_i}	Alice's probability of choosing intensity μ_i
nX^{μ_i}	Detections when both chose basis \boxplus and intensity μ_i
nZ^{μ_i}	Detections when both chose basis \boxtimes and intensity μ_i
mX^{μ_i}	Detections in error for basis \boxplus and intensity μ_i
mZ^{μ_i}	Detections in error for basis \boxtimes and intensity μ_i

B. Key Rate

As we move from the asymptotic case [23] to a real-life scenario with finite key size, the key rate R becomes dependent on the size of the key. According to the modification proposed in [18], adopted from [24]:

$$R_{\text{GLLP}}(\eta) \rightarrow R_{\text{fin}}(\eta_{\text{avg}}, N_{\text{post}}) \quad (2)$$

where η_{avg} is the average transmittance and N_{post} is the number of post-selected signals, obtained by applying threshold transmittance [8] filtering to the total number of pulses (N):

$$\eta_{\text{avg}} = \frac{\int_{\eta_t}^1 d\eta \eta p_{\eta_o, \sigma}(\eta)}{\int_{\eta_t}^1 d\eta p_{\eta_o, \sigma}(\eta)}, \quad N_{\text{post}} = N \int_{\eta_t}^1 d\eta p_{\eta_o, \sigma}(\eta) \quad (3)$$

After postselection, a fraction of $R_{\text{fin}}(\eta_{\text{avg}})$ is left, giving a secure key rate (SKR) of [18]:

$$R_{\text{sec}} = R_{\text{fin}} \times \int_{\eta_t}^1 d\eta p_{\eta_o, \sigma}(\eta) \quad (4)$$

Here, the threshold transmittance is chosen such that the key rate is zero in the region where $\eta < \eta_t$.

The secure key length, ℓ produced from sending N pulses is given as [25]:

$$\ell = s_{X,0} + s_{X,1} - s_{X,1} h(\phi_x) - n_x f_{\text{ec}} h(e_{\text{obs}}) - 6 \log_2 \frac{21}{\epsilon_{\text{sec}}} - \log_2 \frac{2}{\epsilon_{\text{cor}}} \quad (5)$$

The first two terms represent the contributions to the key length from zero-photon and single-photon pulses, respectively. A fraction of the single-photon contribution ($s_{X,1}$) is sacrificed for privacy amplification, as denoted by the *third term*. Here, ϕ_X represents the upper bound of the phase error rate in the rectilinear (\boxplus) basis and serves as the argument for the binary/Shannon entropy, $h(\cdot)$.

The *fourth term* gives the expense for the error correction algorithm. In the \boxplus basis, n_X is the randomly chosen post-processing block size (for all μ_i 's) and m_X is the number of incorrect bits. f_{EC} denotes the error correction efficiency. In this case, the argument of the binary entropy function is the quantum bit error rate ($e_{obs} = \frac{m_X}{n_X}$). Finally, the last two terms account for relatively small errors, such as: probability of non-identical keys slipping through the error verification steps and security leakage in the generated bit. We note that the entire diagonal basis (\boxtimes) is sacrificed between Alice and Bob to bound statistics in the \boxplus basis.

The final SKR is given by $R_{fin} = \frac{\ell}{N}$. This presents an optimization problem, as a lower threshold keeps more signal overall but also keeps signal with lower transmittance, which is more likely to be from noise in the detector. Meanwhile, a higher threshold reduces the amount of errors at the cost of sacrificing a larger portion of the key.

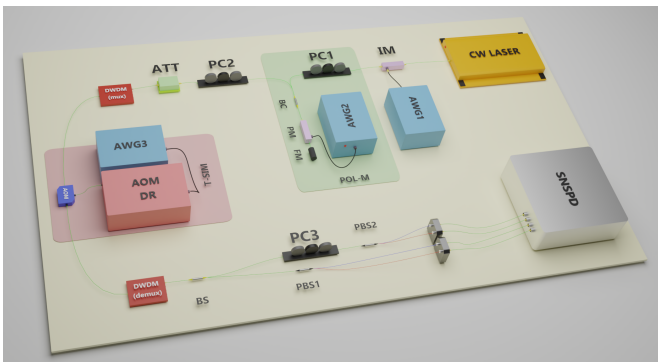


Fig. 1: Experimental setup of BB84 with decoy states. Alice prepares laser pulses using a continuous wave (CW LASER) source and intensity modulator (IM), driven by an arbitrary waveform generator (AWG1). Polarization encoding is done at polarization modulation (POL-M) stage. Optical fiber carrying the signal from one dense wavelength-division multiplexing (DWDM, mux) to other (DWDM, demux) is the quantum channel. The turbulence simulation stage (T-SIM) is to simulate atmospheric effect.

III. EXPERIMENTAL SETUP

Our experimental setup is shown in Fig. 1.

For weak coherent source, we used a low power (2 mW) continuous wave (CW) laser of central wavelength 1550.5 nm with high accuracy ($\pm 2 \times 10^{-5}$ nm). We carved the continuous wave into pulses using a LiNbO₃ based intensity modulator. An arbitrary waveform generator (AWG1) was used to produce signal and decoy states. We used a null point modulator bias

controller device to ensure a stable operation state by applying compensation bias voltage.

We encoded each pulse with a polarization in either the \boxplus or \boxtimes basis (H, D \equiv 0; V, A \equiv 1). Polarization modulation was achieved through the use of a beam circulator (BC), a phase modulator (PM) and a Faraday mirror (FM). The sequence of pulses traveled through a beam circulator and then a phase modulator which modified the phase using short voltage pulses with the help of an arbitrary waveform generator (AWG2). To address any undesired changes in the polarization states due to frequency or polarization mode dispersion, a FM was employed to compensate for any induced phase shift ϕ_e .

After optical attenuation through a combination of a digital and analog attenuators, the pulse train was multiplexed through a dense wavelength division multiplexing (DWDM) device. Upon being demultiplexed with a corresponding DWDM at Bob's side, random basis selection (\boxplus or \boxtimes) was performed with a 50:50 beam splitter (BS) and polarization measurements (\leftrightarrow , \updownarrow or \nearrow , \nwarrow) were performed with polarization beam splitters (PBS). Finally, a superconducting nanowire single photon detector (ID281 SNSPD) sent the detected signal to a time to digital converter (TDC, ID801) which was synced with AWG1, AWG2 and AWG3.

Alice prepares her states by optimizing the decoy state parameters $\{q_x, \mu_1, \mu_2, p_{\mu_1}, p_{\mu_2}\}$ [25] associated with the desired turbulence parameters η_o and σ . The AWG1 uses μ_1 and μ_2 to implement the average intensity of the signal and weak decoy states on the pulses, respectively. The occurrence rates of these two states are controlled by p_{μ_1} and p_{μ_2} in order. The vacuum state intensity, μ_3 is set to zero and the probability of occurrence, p_{μ_3} can be found from the relation: $p_{\mu_1} + p_{\mu_2} + p_{\mu_3} = 1$. The AWG2 controls the probability of Alice choosing either \boxplus or \boxtimes basis, utilizing the parameters q_x and q_z . Note that $q_x + q_z = 1$.

Channel parameters η_o and σ are used to create an arb file for AWG3 to implement log-normally distributed transmittance for the quantum channel using AOM.

The optimized parameter values for 37 dB and 40 dB cases are listed in Table I.

TABLE I: Optimized parameter values obtained for turbulence parameter set $\{\eta_o, \sigma\}$, using the method in [25].

Turbulence	q_x	μ_1	μ_2	p_{μ_1}	p_{μ_2}
37 dB	0.795	0.678	0.293	0.361	0.429
40 dB	0.677	0.701	0.281	0.246	0.490

IV. ANALYSIS

Tables II and III show the critical differences between the old single-photon avalanche detectors (SPAD) used in [20], and the new SNSPD detectors. The dark count rate of the new detectors is almost 2 orders of magnitude lower than that of the old detectors. The SNSPD has a dead time ranging from 70 – 80 ns, whereas our old SPAD detector's dead time is 9.1 μ s. Compared to the old detectors, the after-pulse recovery time of the SNSPD detectors is significantly

smaller. In our experiment, we used a 10 MHz signal, which results in a repetition rate of 100 ns. Consequently, there is no waiting time between two consecutive pulses, whereas the SPAD detectors had a significant recovery period between detections, resulting in lost pulses.

After preparing the setup, we collected 3×10^{10} bits of data (processing time is approximately 50 minutes at the mentioned rate) for analysis. To find the optimized threshold region, we studied the distilled key rate as a function of threshold transmittance η_t for both cases [26]. The result is shown in Fig. 2.

TABLE II: Background-noise parameters comparison between old and new sets of detectors. Background click probability $P_{bg}(\eta) = Y_o + b\eta$. The SNSPD (new) is completely independent on transmittance.

Detector	Y_o^{old} ($\times 10^{-7}$)	Y_o^{new} ($\times 10^{-7}$)	b^{old} ($\times 10^{-4}$)	b^{new} ($\times 10^{-4}$)
\leftrightarrow	76 ± 6	7.1 ± 0.6	2.6 ± 0.4	0
\updownarrow	310 ± 20	6.7 ± 0.6	1.8 ± 0.4	
\nearrow	670 ± 30	6.2 ± 0.6	2.7 ± 0.4	
\searrow	670 ± 30	6.1 ± 0.6	1.8 ± 0.4	

TABLE III: Comparison between old and new device parameters

Experimental Parameters	Old Setup	New Setup
Bob's optical efficiency	0.42 ± 0.02	0.42 ± 0.02
Optical misalignment	0.003 ± 0.002	0.001 ± 0.0004
Quantum efficiency	0.1 ± 0.05	$.8 \pm 0.05$
Dead time	~ 9000 ns	≤ 80 ns
Time jitter	≤ 200 ps	≤ 50 ps

In both situations, we found the optimized threshold lying between the range 2.5×10^{-4} to 3.5×10^{-4} . We chose $\eta_{tc} = 3 \times 10^{-4}$ as the optimum threshold for the next step.

Here we calculated the the SKR as a function of mean channel loss in three different ways. We simulated R_{sec} vs η for both zero cutoff and for optimal cutoff conditions. The simulation graph shows substantial deviation (~ 1.85 dB) for high-loss condition. Our measurement of key rate with considering η_{tc} is very close to the simulation curve in both cases. The possible reasons for the deviation is optical misalignment and fluctuation in the average signal and decoy photon number.

By comparing the simulation and experimental graphs in Figs. 2 and 3, we conclude:

- (i) Using threshold transmittance η_t to discard bits at lower transmittance, we experimentally demonstrated the increment of the key rate beyond 40 dB loss channel as proposed in [8] and demonstrated by our group up to 19 dB [20].
- (ii) The optimum threshold region for maximum key rate is found to be similar for both the 40 dB and 37 dB channels, ranging from 2.5×10^{-4} to 3.5×10^{-4} , and is independent of the channel parameters. This finding supports the P-RTS theory [18]. Our threshold

region is significantly lower (by 2 orders of magnitude) than the previous findings reported in [20], as expected since the new detectors' background click probability P_{bg} is not dependent on transmittance. Moreover, the only contributing parameter to P_{bg} is the background noise Y_o , which is also significantly smaller (by up to 2 orders of magnitude) (see Table I). The P-RTS paper predicts the dependability of η_t only on device parameters, which provides additional evidence in favor of the theory. Interestingly, in our previous work, for the highest tolerated loss at 19 dB, the optimal threshold was found to be sensitive to channel statistics and experienced 40% decrease in SKR with a transmittance threshold optimized for 17 dB.

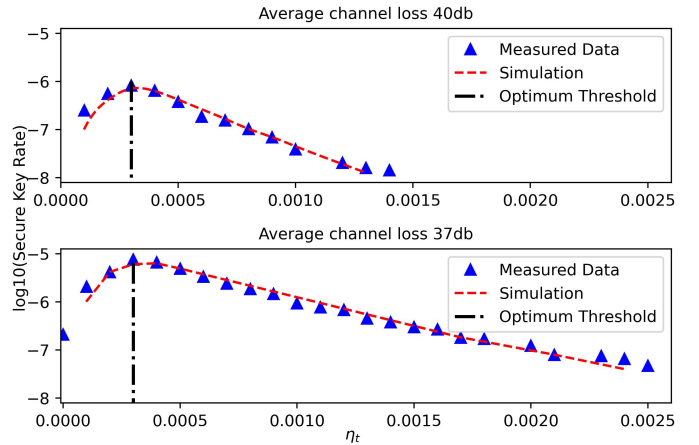


Fig. 2: Finding optimized key rate using ARTS [26] method. The variation in logarithm of the secure key rate for increasing applied transmittance cutoff: For 40 dB mean channel loss (top) and For 37 dB mean channel loss (bottom)

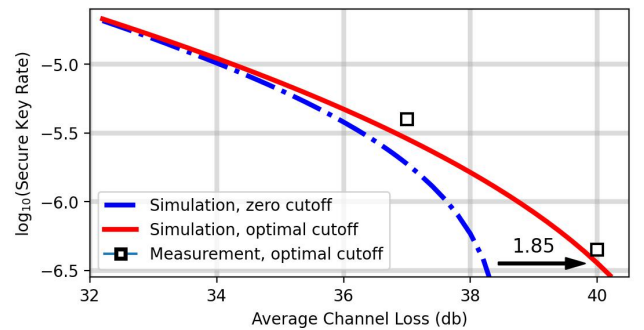


Fig. 3: Simulation and Measurements using P-RTS method: cutoff set at $\eta_{ot} = 3 \times 10^{-4}$, taken from Fig. 2.

V. CONCLUSION

We experimentally simulated a finite-key decoy state BB84 in turbulent, high loss environments, of up to 40 dB, which extended our previous work beyond 19 dB. This was achievable by replacing SPAD detectors with SNSPD detectors with higher efficiency, lower dark count rates and no after pulsing.

This work is especially relevant for free space systems at the ground level, for example at metropolitan scales [15], [16].

We found that at the loss limits of our system, the optimal data rejection threshold was not sensitive to channel statistics, in accordance with the P-RTS theory in [18]. To extend our work, the effect of varying levels of turbulence can be analyzed in the context of P-RTS, which can also include testing higher turbulence levels ($\sigma^2 \gtrsim 1.2$) using the more appropriate gamma-gamma model, as suggested in [19]. Further studies can include experimental testing of other protocols such as measurement device independent quantum key distribution (MDI QKD) [27] over our simulated turbulent channel. An MDI QKD testbed could consider the effect of turbulence on channel asymmetry and its relation to the Hong-Ou-Mandel interferometer visibility at the detection apparatus, as has been investigated theoretically in [18].

ACKNOWLEDGMENTS

We wish to thank B. Qi, E. Moschandreou, and B. Rollick for comments and discussion.

REFERENCES

- [1] C. H. Bennett and G. Brassard, "Quantum cryptography: Public key distribution and coin tossing." Proceedings of IEEE International Conference on Computers, Systems, and Signal Processing, Bangalore, India (IEEE, New York, 1984), pp. 175–179.
- [2] C. H. Bennett, F. Bessette, G. Brassard, L. Salvail, and J. Smolin, "Experimental Quantum Cryptography," *J. Cryptology*, vol. 5, pp. 3-28, 1992.
- [3] D.N. Klyshko, "Photons and Nonlinear Optics," Gordon and Breach Science (New York, 1988).
- [4] O. Benson, C. Santori, M. Pelton, and Y. Yamamoto, "Regulated and Entangled Photons from a Single Quantum Dot," *Phys. Rev. Lett.*, vol. 84, 2513 (2000).
- [5] B. Huttner, N. Imoto, N. Gisin, and T. Mor, "Quantum cryptography with coherent states," *Phys. Rev. A*, vol. 51, 1863, March 1995.
- [6] G. Brassard, N. Lutkenhaus, T. Mor, and B. C. Sanders, "Security aspects of practical quantum cryptography," Conference Digest, International Quantum Electronics Conference, Nice, France, 2000.
- [7] W. Hwang, "Quantum Key Distribution with High Loss: Toward Global Secure Communication," *Phys. Rev. Lett.*, vol. 91, 057901, August 2003.
- [8] C. Erven, B. Heim, E. Meyer-Scott, J. P. Bourgoin, R. Laflamme, G. Weihs, and T. Jennewein, "Studying free-space transmission statistics and improving free-space quantum key distribution in the turbulent atmosphere," *New J. Phys.*, vol. 14, 123018, December 2012.
- [9] N. Lütkenhaus, "Security against individual attacks for realistic quantum key distribution," *Phys. Rev. A*, vol. 61, 052304, April 2000.
- [10] S.-K. Liao *et al.*, "Satellite-to-ground quantum key distribution," *Nature*, vol. 549, pp. 43-47, 2017.
- [11] S.-K. Liao *et al.*, "Long-distance free-space quantum key distribution in daylight towards inter-satellite communication," *Nature Photonics*, vol. 11, pp. 509-513, 2017.
- [12] J.-Y. Wang *et al.*, "Direct and full-scale experimental verifications towards ground-satellite quantum key distribution," *Nature Photonics*, vol. 7, pp. 387-393, 2013.
- [13] D. Rosenberg *et al.*, "Practical long-distance quantum key distribution system using decoy levels," *New Journal of Physics*, vol 11, 045009, 2009.
- [14] T. Miya *et al.*, "Ultimate Low-loss Single-mode Fibre at 1.55 μm ," *Electronics Letters*, vol. 15, pp. 106-108, February 1979.
- [15] A. Kržič *et al.*, "Metropolitan free-space quantum networks," arXiv preprint, arXiv:2205.12862, 2022.
- [16] S. K. Liao *et al.*, "Satellite-to-ground quantum key distribution," *Nature*, vol. 549, pp. 43–47, August 2017.
- [17] A. K. Majumdar and J. C. Ricklin, "Free-Space Laser Communications: Principles and Advances," Springer-Verlag New York, 2008.
- [18] W. Wang, F. Xu, and H.-K. Lo, "Prefixed-threshold real-time selection method in free-space quantum key distribution", *Phys. Rev. A*, vol. 97, 032337, March 2018.
- [19] M. A. Al-Habash, L. Andrews, and R. L. Philips, "Mathematical model for the irradiance probability density function of a laser beam propagating through turbulent media," *Optical Engineering*, vol. 40, pp. 1554-1562, August 2001.
- [20] E. Moschandreou, B. J. Rollick, B. Qi, and G. Siopsis, "Experimental decoy-state Bennett-Brassard 1984 quantum key distribution through a turbulent channel," *Phys. Rev. A*, vol. 103, 032614, March 2021.
- [21] F. Kullander and L. Sjöqvist, "Effects of turbulence on a combined 1535-nm retro reflective and a low-intensity single-path 850-nm optical communication link," *Proceedings of SPIE - The International Society for Optical Engineering*, vol. 6399, 2006.
- [22] J. A. Louthain and J. D. Schmidt, "Integrated approach to airborne laser communication," *Proc. of SPIE*, vol. 7108, 71080F-1, 2008
- [23] D. Gottesman, H.-K. Lo, N. Lütkenhaus, and J. Preskill, "Security of quantum key distribution with imperfect devices," *International Symposium on Information Theory*, 2004.
- [24] M. Tomamichel, C. C. W. Lim, N. Gisin, and R. Renner, "Tight finite-key analysis for quantum cryptography". *Nat. Commun.*, vol. 3, 634, January 2012.
- [25] C. C. W. Lim, M. Curty, N. Walenta, F. Xu, and H. Zbinden, "Concise security bounds for practical decoy-state quantum key distribution," *Phys. Rev. A*, vol. 89, 022307, February 2014.
- [26] G. Vallone, D. G. Marangon, *et al.*, "Adaptive real time selection for quantum key distribution in lossy and turbulent free-space channels", *Phys. Rev. A* vol. 91, 042320, April 2015.
- [27] H.-K. Lo, M. Curty, and B. Qi, "Measurement-Device-Independent Quantum Key Distribution", *Phys. Rev. Lett.*, vol. 108, 130503, March 2012.